2026 IEEE International Conference on Robotics and Automation (ICRA 2026)
June 1-5, 2026. Vienna, Austria

A Novel Paddling Propulsion Gait for a Wheel-Legged Robot on Sand Terrain

En-Chieh Tsui[1], Wei-Ting Chen[1], Wei-Shun Yu[1],
Hung-Hsin Chen[2], Shaoyu Chien[2], and Pei-Chun Lin[1]*, *Senior Member, IEEE*

***Abstract*—Autonomous Mobile Robots are typically limited to structured environments, as conventional wheeled propulsion often fails on deformable terrains like sand due to excessive wheel slip and sinkage. To address this mobility challenge, this paper introduces a novel locomotion strategy for a high-degree-of-freedom wheel-legged robot. The proposed method is a gait based on an asymmetric "dynamic compact-and-push" cycle, where the robot's limbs perform a paddling-like motion to actively remodel the granular media. This active terrain remodeling allows the robot to generate net forward thrust where conventional wheeled locomotion is ineffective. We systematically designed and experimentally validated four distinct gaits founded on this principle. The results demonstrate that this approach enables sustained forward motion in an environment where wheeled propulsion is verified to fail, with the asynchronous paddling gait proving most effective. This work contributes a new, validated locomotion mechanism for sand terrains and provides a quantitative comparison of different limb coordination strategies.**

***Index Terms*—Wheel-legged Robot, Gait Design, Locomotion, Sand Terrain.**

I. INTRODUCTION

Autonomous Mobile Robots have become integral to structured indoor environments like warehouses and factories, where they operate on artificial, continuous surfaces to boost intralogistics efficiency [1]. However, the expansion of robotics into outdoor and unstructured settings—such as planetary exploration [2], agriculture [3], and search and rescue [4]—demands robots that can reliably navigate deformable terrains like sand and mud. On such terrains, conventional wheeled robots face significant mobility challenges, as high wheel slip and sinkage prevent effective propulsion [5]–[7]. In severe cases, this can lead to complete immobilization, a state often defined as "entrapment" [8]. This mobility issue is not trivial; it was the cause of the Spirit rover's mission end on Mars [2].

Historically, approaches to enhance vehicle mobility on sand have focused on optimizing the vehicle's internal state within a wheeled locomotion paradigm. These strategies include modifying wheel-soil interaction models based on terramechanics [9], adjusting power distribution to minimize slippage [10], or using active suspension to shift the center of gravity. Tracked vehicles, like FUMA, inherently offer better traction due to a larger contact area but their fundamental interaction with the terrain remains that of a surface-driven vehicle [4], [11]. These conventional methods treat the terrain as an unchangeable obstacle and are fundamentally limited once wheeled or tracked propulsion becomes ineffective.

To overcome these limitations, research has shifted towards robots with higher degrees of freedom (DOF), such as legged and wheel-legged hybrids. Legged robots, like BigDog [12], and modern learning-based quadrupeds [13]–[15], have demonstrated remarkable agility on complex terrains. Their control strategies often focus on sophisticated gait planning to maintain stability and efficiency during forward locomotion, sometimes even learning to adapt to deformable ground by feeling its properties [14], [16]. Similarly, wheel-legged hybrids like Wheel Transformer [17], Quattroped [18] or TurboQuad [19] offer versatility by switching between modes. While much of this research targets efficient traversal over varied but generally firm ground, the specific challenge of generating sustained propulsion on soft, flowable media like sand, where traditional wheels fail, remains a key area of investigation.

A few pioneering studies have begun to explore "active terrain remodeling" as a primary locomotion strategy. Shrivastava et al. demonstrated that a rover could use unconventional gaits to "swim" through granular media [8]. Qi et al. proposed a worm-inspired creeping gait that varies its wheelbase to adapt to terrain resistance [16]. These works are grounded in the principles of terradynamics, the study of force generation on bodies moving within flowable ground [20]. Further studies in this domain have revealed that the specific design and kinematics of a robot's appendages are critical for effectively generating propulsive forces in such media [21]. This understanding allows for a paradigm shift: treating the terrain not as an obstacle, but as a manipulable medium where motion can be generated by strategically interacting with it.

This paper builds upon this emerging paradigm. Leveraging a high-DOF wheel-legged platform, previously shown capable of multi-terrain mobility including stair-climbing [5], we introduce a novel laterally-based gait designed specifically for locomotion on sand. The core of our strategy is an asymmetric "dynamic compact-and-push" cycle. By coordinating the hip, steering, and wheel motors, the robot's limbs execute a paddling-like motion. During the recovery stroke of a lateral sweep, the wheels actively displace and compact the loose sand. In the subsequent propulsive stroke, the wheels engage with this freshly compacted, firmer ground to generate

This work was supported by the DELTA ELECTRONICS INC., Taiwan, under Contracts TW.2026.0040.

*Corresponding author: Pei-Chun Lin (email:peichunlin@ntu.edu.tw)
[1]Department of Mechanical Engineering, National Taiwan University, Taipei 10617, Taiwan.
[2]DELTA ELECTRONICS INC., Taiwan.

effective traction. This periodic cycle creates a net forward thrust, enabling the robot to achieve sustained forward motion where conventional wheeled propulsion is ineffective. The main contributions of this paper are:

1) **A novel propulsion mechanism for sand terrain:** We introduce and formalize a laterally-based gait founded on a "dynamic compact-and-push" cycle, which enables a robot to generate net forward displacement by actively remodeling the terrain.
2) **Systematic gait design and analysis:** We systematically design and compare four distinct gait variations based on this principle, analyzing their theoretical advantages in terms of propulsive force, stability, and energy efficiency.
3) **Rigorous experimental validation:** Through physical experiments on a granular testbed, we provide a quantitative comparison of the propulsive effectiveness of the four gait designs, validating our approach and identifying the most effective strategy based on metrics of forward displacement and Cost of Transport (COT) [22].

The remainder of this paper is organized as follows. Section II describes the robot platform architecture and kinematic modeling. Section III details the design of the laterally-based propulsion gaits. Section IV presents the experimental validation and analyzes the results. Finally, Section V concludes the paper and discusses future work.

II. PLATFORM ARCHITECTURE AND KINEMATIC MODELING

A. Platform Architecture

The robotic platform central to this research inherits its fundamental hardware architecture from a versatile wheel-legged hybrid system previously developed for multi-terrain traversal [5].As illustrated in Fig. 1, the platform is composed of a central body and four identical limbs. Each limb possesses three active DOFs and one passive DOF, resulting in a total of 12 active and 4 passive DOFs for the entire platform. The active DOFs for each limb are: one rotational DOF at the hip joint $\theta_{1,\,i,\,i=1\sim4}$ for lateral swinging, one rotational DOF at the steering mechanism $\theta_{2,\,i,\,i=1\sim4}$, and one rotational DOF for the hub motor wheel $\omega_{3,\,i,\,i=1\sim4}$. The passive DOF is provided by a linear suspension spring within each leg. It is the specific synergy between these DOFs—particularly the active hip rotation and independent steering—that forms the mechanical foundation for the novel, laterally-based propulsion gait presented in this paper. While the platform can operate as a four-wheel independent drive and steering (4WID-4WIS) vehicle, this work creatively repurposes its articulated "legged" capabilities to enable locomotion on sand.

The capacity to execute our "dynamic compact-and-push" cycle is directly enabled by two key mechatronic designs, detailed in Fig. 2:

1) **High-Torque Hip Actuation for Terrain Remodeling**: As shown in Fig. 2(a), each hip joint is actuated by a worm gear mechanism. The primary advantage of this design is its large gear reduction ratio, which provides the high torque necessary to overcome the significant resistive forces encountered when paddling through granular media. Furthermore, the inherent non-backdrivable feature of the worm gear provides substantial holding torque against external loads. While our dynamic gaits do not have a static stance phase, this characteristic ensures robust trajectory tracking by preventing the reaction forces from the sand from back-driving the mechanism. This allows the robot to execute the powerful compact-and-push maneuver with high fidelity, which is critical for the success of our locomotion strategy.
2) **Multi-Functional Wheel-Legged Module**: The wheel-legged module, depicted in Fig. 2(b), integrates a hub motor, a steering motor, and the passive suspension system. Crucially, by employing a spline mechanism, the steering actuation is successfully decoupled from the vertical suspension travel. This design grants each wheel-leg independent driving and steering capabilities. The independent steering DOF (θ_2) is the prerequisite for transforming the wheel into an active "paddle" for displacing and compacting sand laterally. Simultaneously, the independent hub motor (ω_3) provides immediate propulsion the moment the wheel tread engages with the freshly compacted ground.

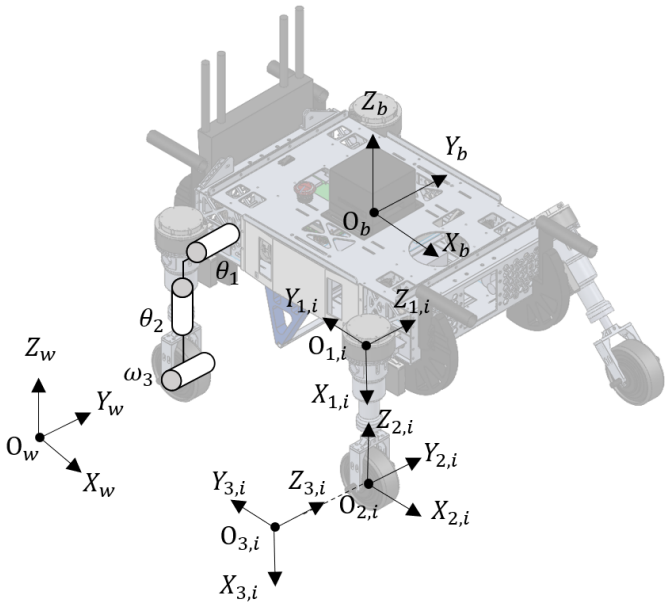

Fig. 1. The wheel-legged robot platform. The world coordinate system is $\{O_w - X_w Y_w Z_w\}$, and the body coordinate system attached to its geometric center is $\{O_b - X_b Y_b Z_b\}$. Each limb has three active DOFs: hip rotation θ_1, steering rotation θ_2, and wheel rotation ω_3.

B. Kinematic Modeling

To formulate and command the proposed gaits, we define two primary coordinate systems as shown in Fig. 1. The fixed world coordinate system is denoted by $\{O_w - X_w Y_w Z_w\}$,

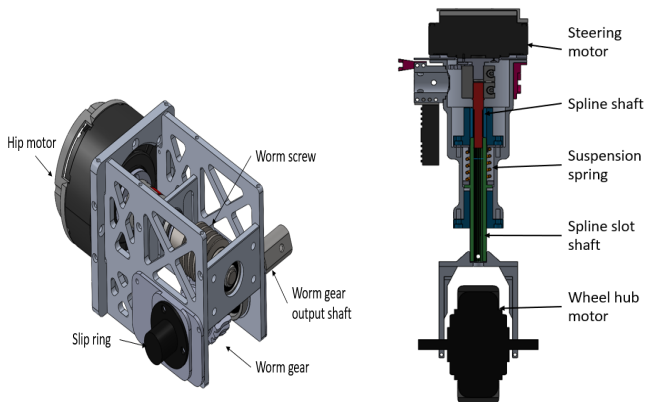

(a) Hip joint module (b) Wheel-leg module

Fig. 2. Key mechanical designs of the platform. (a) The hip module's worm gear provides self-locking capability. (b) The wheel-legged module's spline shaft decouples steering from suspension.

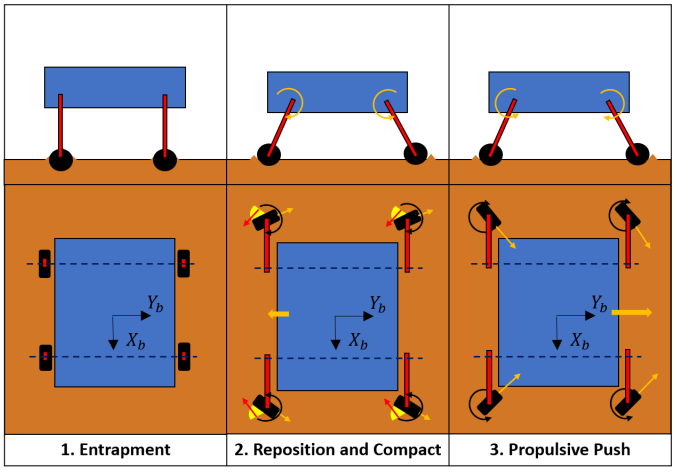

Fig. 3. Conceptual illustration of the two-phase propulsion generation sequence. The first row shows the side view and the second row shows the top view of the robot's motion. During the 'Reposition and Compact' phase, the wheel creates a firmer surface. Subsequently, in the 'Propulsive Push' phase, the wheel gains effective traction on this newly compacted ground, generating significant forward motion.

while the moving coordinate system at the robot's geometric center is denoted by $\{O_b - X_bY_bZ_b\}$. We assume the robot's center of mass coincides with the origin O_b.

Based on rigid body kinematics, the linear velocity of the center of each wheel, $\vec{V}_{\text{i, i=1}\sim4}$, in the body frame can be derived from the angular velocities of the hip joint $\dot{\theta}_{1,i}$ and the wheel hub motor $\omega_{3,i}$, given the joint angles of the hip $\theta_{1,i}$ and steering $\theta_{2,i}$. For each wheel $i \in \{1, 2, 3, 4\}$, the velocity vector is given by:

$$\vec{V}_i = \begin{bmatrix} V_{x,i} \\ V_{y,i} \\ V_{z,i} \end{bmatrix} = \begin{bmatrix} -\dot{\theta}_{1,i} L_{ext} \sin\theta_{1,i} + \omega_{3,i} r_{wheel} \cos\theta_{2,i} \\ \omega_{3,i} r_{wheel} \sin\theta_{2,i} \\ \dot{\theta}_{1,i} L_{ext} \cos\theta_{1,i} \end{bmatrix} \tag{1}$$

where L_{ext} is the distance from the hip's rotational axis to the wheel's center, and r_{wheel} is the wheel radius.

The linear velocity of the body's center of mass, $\vec{V}_b$, is the average of the four wheel center velocities:

$$\vec{V}_b = \frac{1}{4} \sum_{i=1}^{4} \vec{V}_i \tag{2}$$

Furthermore, the angular velocity of the body, $\vec{\omega}_b$, can be obtained by relating the linear velocities of the wheel centers to their position vectors relative to the body's center of mass, $\vec{r}_i$:

$$\vec{V}_i = \vec{V}_b + \vec{\omega}_b \times \vec{r}_i \tag{3}$$

By solving this system of equations for all four wheels, the body's linear velocity $\vec{V}_b$ and angular velocity $\vec{\omega}_b$ can be fully determined. This kinematic model provides the foundation to translate high-level gait parameters into precise motor commands.

III. LOCOMOTION GAIT DESIGN FOR SAND TERRAIN

A. Motivation: Failure of Wheeled Locomotion

The efficiency of wheeled locomotion on soft terrain is closely related to the slip ratio, s [10].When the tractive force of the wheels exceeds the adhesion provided by the ground, slip occurs, leading to energy waste and reduced displacement.The longitudinal slip ratio is defined as:

$$s = 1 - \frac{v}{\omega_3 \cdot r_{\text{wheel}}} \tag{4}$$

where v is the actual forward linear velocity of the wheel's center, ω_3 is the wheel's angular velocity, and r_{wheel} is the wheel radius. A slip ratio of $s = 1$ indicates that the wheel is spinning without generating any forward motion. On deformable terrains like sand, high slip ($s \to 1$) and sinkage lead to a complete loss of mobility. In this study, we confirm experimentally that conventional wheeled motion results in slip ratios exceeding 80%, a state of mobility failure we term "entrapment" [6]. This failure motivates the development of an alternative locomotion strategy.

B. Principle of Propulsion via Dynamic Compaction

Instead of relying on conventional wheeled propulsion, our approach is to actively remodel the surrounding terrain to generate thrust. We treat the granular media not as a static obstacle, but as a manipulable medium. This "remodeling" is achieved through an asymmetric "dynamic compact-and-push" cycle, which prepares a high-traction path for propulsion, as illustrated in Fig. 3. The cycle, initiated from a high-slip state, consists of two primary phases(Reposition and Compact,Propulsive Push):

1) **Entrapment:** The robot is in a static, high-slip state, with its wheels sunken into the sand and unable to generate effective traction through conventional rotation.
2) **Reposition and Compact:** A limb swings laterally outwards (abduction). During this phase, the angled wheel actively displaces and compacts the surrounding loose sand. The reaction force generated by displacing

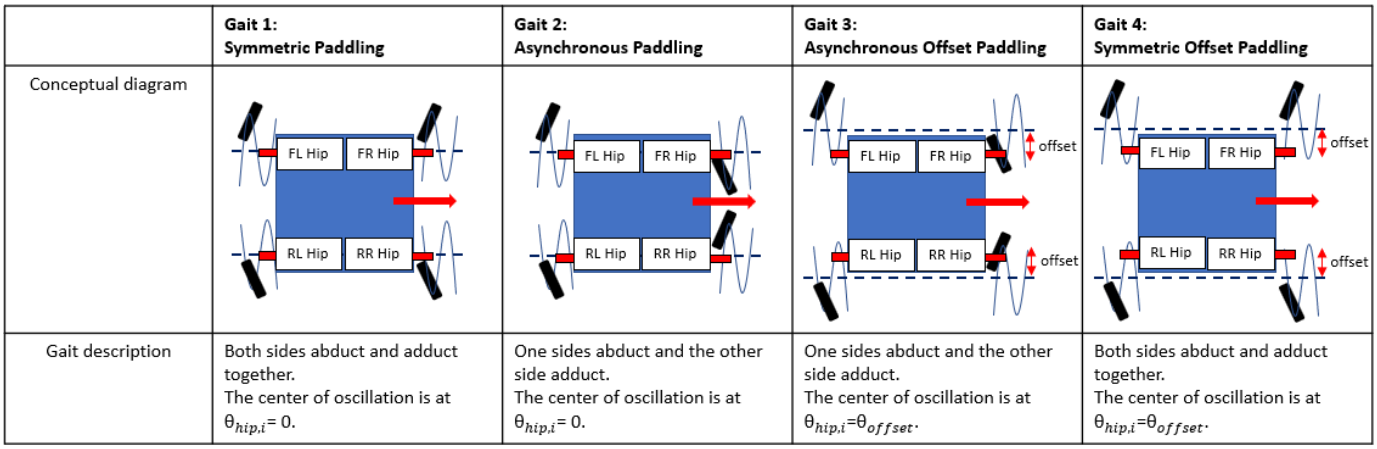

Fig. 4. The four propulsion gait designs, illustrating the conceptual diagrams and coordination patterns.

this sand causes a slight backward movement of the robot. However, the primary outcome of this phase is the creation of a small, localized region of densified, firmer ground.

3) **Propulsive Push:** The limb then swings laterally inwards (adduction), driving the wheel against the freshly compacted surface created in the previous phase. Pushing against this firm ground provides significantly higher traction, generating a strong forward propulsive force that moves the robot's body forward.

The key to achieving net forward locomotion lies in this engineered asymmetry. The large forward thrust generated during the propulsive push on compacted sand consistently overcomes the minor backward reaction force from the repositioning phase on loose sand, resulting in sustained net forward progress.

C. Sand Terrain Propulsion Gait Design

Based on this principle, we designed four distinct gaits to investigate how different limb coordination patterns affect propulsive efficiency and stability. All gaits ensure that the absolute angle of the joints of the left and right hips ($|\theta_{1,L}| = |\theta_{1,R}|$) remains the same at all times to prevent unwanted body rotation. The design rationale and kinematic patterns are summarized in Fig. 4.

- **Gait 1: Symmetric Paddling:** The hypothesis is that synchronized limb motion concentrates reaction forces in the sagittal plane, generating the maximum net forward thrust.
- **Gait 2: Asynchronous Paddling:** This gait introduces a 180° phase offset between the left and right sides to maintain a large support polygon, aiming to improve overall dynamic stability.
- **Gait 3: Asynchronous Offset Paddling:** Building upon Gait 2, this gait incorporates an asymmetric offset in the hip's center of oscillation, hypothesized to improve forward progression for asynchronous motion.
- **Gait 4: Symmetric Offset Paddling:** This gait applies a symmetric outward offset to the center of oscillation. The hypothesis is that this reduces the instability risk associated with Gait 1 by consistently maintaining a wider support base.

D. Control Implementation

To execute the designed gaits, we define the joint trajectories as parameterized motion primitives. For a given limb i, the position commands for the hip and steering joints are formulated using sinusoidal functions. The hip angle command, $\theta_{1,i}(t)$, is determined by an amplitude A_{hip}, an offset of the oscillation center O_{hip}, and a frequency f:

$$\theta_{1,i}(t) = O_{\text{hip}} + A_{\text{hip}} \sin(2\pi f t + \frac{\pi}{2}) \tag{5}$$

Simultaneously, the steering angle command, $\theta_{2,i}(t)$, is synchronized with the hip motion to function as a paddle. It oscillates around $\pi/2$ rad (90 degrees) to ensure the wheel is perpendicular to the motion direction at maximum hip adduction/abduction:

$$\theta_{2,i}(t) = \frac{\pi}{2} + \frac{\pi}{2} \sin(2\pi f t - \frac{\pi}{2}) \tag{6}$$

A key control feature is the coupling of the wheel's rotational velocity to the hip's angular velocity. The objective of this coupling, which we term Tangential Velocity Matching, is to maximize the propulsive effect of the paddling motion.

By commanding the wheel's angular velocity, $\omega_{3,i}(t)$, to synchronize with the tangential velocity, $V_{\text{hip}}(t)$, induced by the hip rotation at the ground contact point (as depicted in Fig. 5), we aim to ensure the wheel acts as a cohesive 'paddle'. This coordinated motion allows the wheel surface to actively shear and compact the granular media in concert with the sweeping leg action. The goal is to convert the wheel's rotational energy into effective work for propulsion, rather than dissipating it through futile churning.

The instantaneous lever arm, L_{cal}, from the hip's center of rotation to the wheel's ground contact point is:

$$L_{\text{cal}} = \sqrt{L_{\text{ext}}^2 + r_{\text{wheel}}^2 + 2L_{\text{ext}} r_{\text{wheel}} \cos(\theta_{1,i})} \tag{7}$$

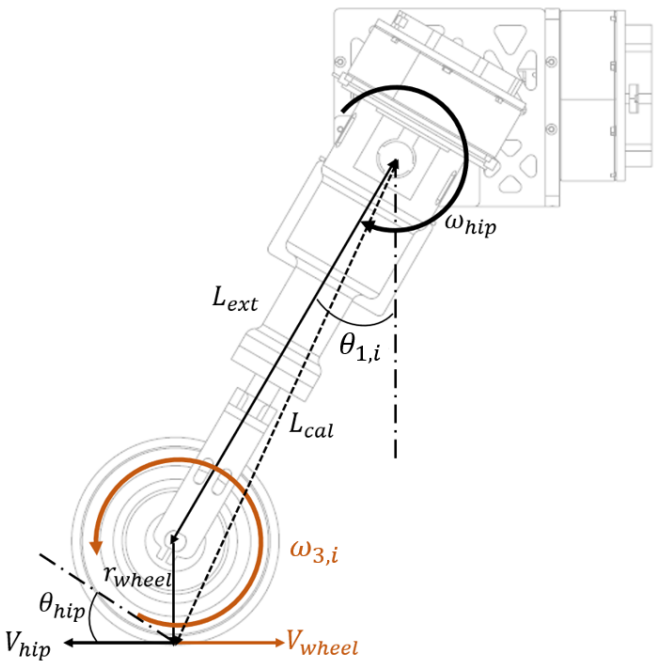

Fig. 5. Kinematic diagram illustrating the tangential velocity matching between the hip angular velocity ($\dot{\theta}_{1,i}$) and the required wheel angular velocity ($\omega_{3,i}$) to maximize propulsive work at the ground contact point.

where L_{ext} is the leg length and r_{wheel} is the wheel radius. The hip's angular velocity is the derivative of Eq. (5):

$$\dot{\theta}_{1,i}(t) = 2\pi f A_{\text{hip}} \cos(2\pi f t) \tag{8}$$

Thus, the horizontal tangential velocity at the contact point is:

$$V_{\text{hip}}(t) = \dot{\theta}_{1,i}(t) L_{\text{cal}} \cos(\theta_{1,i}) \tag{9}$$

The linear velocity from the wheel's rotation is $V_{\text{wheel}}(t) = \omega_{3,i}(t) r_{\text{wheel}}$. By matching these tangential velocities ($V_{\text{hip}} = V_{\text{wheel}}$), we derive the required angular velocity command for the hub motor, $\omega_{3,i}(t)$:

$$\omega_{3,i}(t) = \frac{\dot{\theta}_{1,i}(t) L_{\text{cal}} \cos(\theta_{1,i})}{r_{\text{wheel}}} \tag{10}$$

IV. EXPERIMENTAL VALIDATION AND ANALYSIS

To physically validate the proposed gaits and quantitatively compare their performance, a series of experiments were conducted. The experimental setup is shown in Fig. 6. A rectangular testbed measuring 2 m × 1 m was filled with fine-grained sand to a depth of approximately 10 cm to simulate a natural deformable terrain.

A. Experimental Setup

A Vicon motion capture system was utilized to record the ground-truth trajectory and six-DOF pose of the robot's body. This provided precise data for analyzing displacement, velocity, and body stability. Simultaneously, onboard sensors were used to gather critical operational data: wheel speeds were acquired from hub motor encoders to calculate the slip ratio, and motor currents were collected to evaluate the energy consumption for each gait.

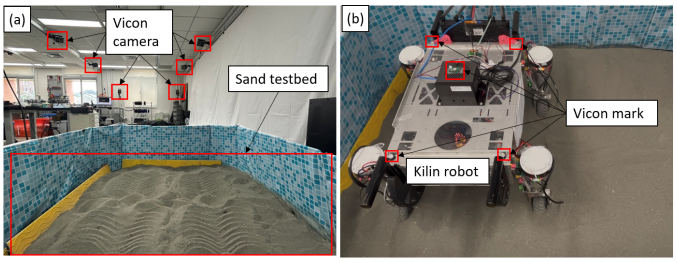

Fig. 6. Experimental setup. (a): The sand testbed surrounded by Vicon motion capture cameras. (b): The robot with Vicon markers attached to its body for precise tracking.

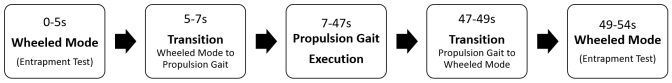

Fig. 7. The standardized 54-second timeline for each experimental run.

B. Experimental Procedure and Metrics

In this study, four distinct gaits were experimentally validated, with the hip oscillation amplitude serving as the primary control variable. Table I summarizes all experimental configurations. Each combination of a gait and its parameter set was executed three times to ensure repeatability.

The experimental procedure for each run followed a standardized 54-second timeline, as illustrated in Fig. 7. To create a challenging initial condition, the robot was placed in the sand testbed with its wheels partially sunk (approximately 5 cm deep). The robot then executed the following sequence:

1) **Wheeled Mode Test (0–5s):** The robot was commanded to drive forward in its conventional wheeled mode. This step was to quantitatively verify the ineffectiveness of wheeled locomotion on this terrain.
2) **Transition to Gait (5–7s):** A 2-second period to transition to the gait's starting posture.
3) **Gait Execution (7–47s):** The designated propulsion gait was executed for a fixed duration of 40 seconds.
4) **Transition to Wheel Mode (47–49s):** A 2-second period to transition back to a wheeled configuration.
5) **Post-Gait Wheeled Mode Test (49–54s):** The robot again attempted to drive forward to test if its new position allowed for effective wheeled locomotion.

To quantitatively compare the four gaits, the following performance metrics were defined based on data from the 40-second execution phase (7–47s):

- **Propulsive Performance:** Measured as the net forward displacement (along the body's Y-axis).
- **Motion Stability:** Quantified by the standard deviation of the robot's body pitch and roll angles.
- **Energy Efficiency:** Assessed using the Cost of Transport (COT), a dimensionless metric calculated as:

$$COT = \frac{E}{mgd} \tag{11}$$

TABLE I
EXPERIMENTAL PARAMETERS FOR PROPULSION GAITS

Propulsion Gait	Experiment Parameters	
	A_{hip} (rad)	O_{hip} (rad)
Gait 1: Symmetric Paddling	0.3	0
	0.4	0
Gait 2: Asynchronous Paddling	0.3	0
	0.4	0
Gait 3: Asynchronous Offset	0.3	0.1
	0.4	0.1
Gait 4: Symmetric Offset	0.3	0.1
	0.4	0.1

TABLE II
AVERAGED SLIP RATIOS IN WHEELED MODE BEFORE AND AFTER GAIT EXECUTION

Gait	Experiment Parameters		0–5s Avg. Slip Ratio (%)	49–54s Avg. Slip Ratio (%)
	A_{hip} (rad)	O_{hip} (rad)		
Gait 1	0.3	0	86.2	96.9
	0.4	0	88.1	96.2
Gait 2	0.3	0	91.2	100
	0.4	0	92.5	92.7
Gait 3	0.3	0.1	98.5	97.5
	0.4	0.1	84.7	97.6
Gait 4	0.3	0.1	92.5	95.4
	0.4	0.1	85.0	96.2

where E is the total electrical energy consumed, m is the robot's mass, g is gravitational acceleration, and d is the net forward displacement.

C. Results and Discussion

1) Verification of Wheeled Locomotion Failure: Table II summarizes the slip ratio analysis. The average slip ratio during the initial 5-second wheeled mode test consistently exceeded 84% for all configurations. This quantitatively confirms that conventional wheeled locomotion is ineffective on the prepared sand terrain, validating the need for an alternative strategy.

Furthermore, the slip ratio in the subsequent post-gait wheeled mode test also remained high (generally >92%). This pair of results provides a critical insight. The consistently high slip ratios, both before and after gait execution, strongly demonstrate that the sand terrain itself renders conventional wheeled motion ineffective. Crucially, the fact that the robot achieved significant net displacement (as detailed in Section IV-C-2) under these exact high-slip conditions serves as direct proof of our proposed gait's effectiveness. It validates that our method is not merely an escape maneuver, but a viable locomotion strategy capable of generating propulsion in an environment where wheels inherently fail.

2) Propulsive Performance of Gaits: The primary metric for gait effectiveness is the net forward displacement (Y-direction). Table III details the results. Gait 2 (Asynchronous Paddling) with a larger amplitude A_{hip}=0.4 rad achieved the maximum average forward displacement of 483.79 mm. This suggests that the out-of-phase motion is highly effective for propulsion. In contrast, Gait 1 (Symmetric Paddling) with A_{hip}=0.4 rad yielded a significantly lower displacement of 313.34 mm. This result contradicts our initial hypothesis that synchronized motion would produce the maximum thrust, indicating that complex soil interaction dynamics dominate the outcome. A clear trend observed across all four gaits is that a larger hip oscillation amplitude leads to a significant increase in forward displacement.

TABLE III
AVERAGED DISPLACEMENT ANALYSIS: Y (FORWARD) AND X (LATERAL) DIRECTIONS

Gait	Experiment Parameters		Y Displacement		X Displacement	
	A_{hip} (rad)	O_{hip} (rad)	Avg. (mm)	Std. Dev. (mm)	Avg. (mm)	Std. Dev. (mm)
Gait 1	0.3	0	164.131	35.51	2.00	34.11
	0.4	0	313.34	33.41	22.40	16.95
Gait 2	0.3	0	173.30	16.96	36.00	4.26
	0.4	0	483.79	97.87	64.80	34.40
Gait 3	0.3	0.1	213.16	11.36	12.00	28.86
	0.4	0.1	316.13	10.22	-4.80	24.22
Gait 4	0.3	0.1	215.48	23.41	32.00	6.11
	0.4	0.1	345.38	41.16	30.80	14.42

TABLE IV
BODY ATTITUDE STABILITY ANALYSIS: PITCH AND ROLL

Gait	Experiment Parameters		Avg.		Std. Dev.	
	A_{hip} (rad)	O_{hip} (rad)	Pitch (deg)	Roll (deg)	Pitch (deg)	Roll (deg)
Gait 1	0.3	0	0.93	-0.30	0.19	0.10
	0.4	0	1.20	-0.65	0.38	0.75
Gait 2	0.3	0	0.81	0.90	0.09	0.19
	0.4	0	1.36	1.10	0.29	0.15
Gait 3	0.3	0.1	1.40	0.32	0.35	0.19
	0.4	0.1	1.09	-0.23	0.24	0.46
Gait 4	0.3	0.1	0.55	-0.15	0.16	0.10
	0.4	0.1	0.94	0.39	0.04	0.11

3) Motion Stability: To assess motion stability, we analyzed the standard deviations of the body pitch and roll angles. Table IV details these results. The data reveals that all gaits maintained a high degree of stability, with average pitch and roll magnitudes remaining below 1.4 degrees. This validates the control constraint of maintaining equal absolute hip angles ($|\theta_{1,L}| = |\theta_{1,R}|$) as an effective method for preventing significant body roll.

Gait 4 (Symmetric Offset Paddling) with A_{hip}=0.3 rad demonstrated the best overall stability, recording an average pitch of only 0.55 degrees and the lowest standard deviation in roll (0.10 deg). This supports the hypothesis that a symmetric outward offset helps maintain a consistently wide and stable support base.

4) Energy Efficiency: Finally, we evaluated the energy efficiency using the COT. The results are presented in Table V. As expected, a larger oscillation amplitude requires a higher total energy expenditure. Notably, for a given amplitude, the total energy consumed across the four gaits is remarkably similar. This implies that the significant differences observed in COT are driven primarily by the variation in effective forward displacement, rather than the energy cost of the motion itself.

Gait 2 (Asynchronous Paddling) with A_{hip}=0.4 rad, which produced the greatest displacement, also exhibited the lowest COT (0.35), making it the most energy-efficient strategy

TABLE V
ENERGY EFFICIENCY ANALYSIS: AVERAGED ENERGY AND COT

Gait	Experiment Parameters		Avg.		Std. Dev.	
	A_{hip} (rad)	O_{hip} (rad)	Energy (J)	COT	Energy (J)	COT
Gait 1	0.3	0	42.08	0.85	0.70	0.22
	0.4	0	50.03	0.51	0.28	0.05
Gait 2	0.3	0	42.00	0.78	1.43	0.08
	0.4	0	51.39	0.35	0.73	0.06
Gait 3	0.3	0.1	43.01	0.64	0.33	0.03
	0.4	0.1	51.19	0.52	0.03	0.03
Gait 4	0.3	0.1	42.13	0.63	0.50	0.06
	0.4	0.1	49.93	0.46	0.83	0.05

overall. This is a significant finding, as it suggests that the most propulsively effective gait is also the most economical. Conversely, Gait 1 (Symmetric Paddling) with A_{hip}=0.3 rad was the least efficient, with a COT of 0.85, due to its small displacement which heavily penalizes the COT calculation. These results indicate that for a combined objective of maximizing both speed and endurance, Gait 2 is the superior choice.

V. CONCLUSION AND FUTURE WORK

This paper introduced a novel locomotion strategy for a high-DOF wheel-legged robot, enabling sustained forward movement on sand terrain where conventional wheeled propulsion fails. We presented the design, analysis, and rigorous experimental validation of four gaits based on a "dynamic compact-and-push" principle, which actively remodels the granular media to generate thrust. The experimental results quantitatively demonstrated the effectiveness of this approach, with all gaits successfully generating propulsion in a verified high-slip environment (slip ratio$>$84%). Notably, we identified that an asynchronous paddling gait with a large amplitude not only produced the maximum forward displacement (483.79 mm) but also proved to be the most energy-efficient, with the lowest Cost of Transport (0.35). This work contributes a new, validated locomotion mechanism for sand terrains and provides a quantitative comparison of different limb coordination strategies, offering valuable insights for the design of future rovers operating in challenging environments.

Building upon the effectiveness of this open-loop implementation, our future work will focus on developing a unified, learning-based control policy. By leveraging high-fidelity simulation and rich proprioceptive feedback, this policy could enable the system to autonomously perceive and adapt to complex environmental interactions, achieving a new level of resilience and robust mobility in unstructured terrains.

REFERENCES

[1] R. Keith and H. M. La, "Review of autonomous mobile robots for the warehouse environment," *arXiv preprint arXiv:2406.08333*, 2024.

[2] A. Seeni, B. Schäfer, and G. Hirzinger, "Robot mobility systems for planetary surface exploration–state-of-the-art and future outlook: a literature survey," *Aerospace Technologies Advancements*, vol. 492, pp. 189–208, 2010.

[3] X. Gao, J. Li, L. Fan, Q. Zhou, K. Yin, J. Wang, C. Song, L. Huang, and Z. Wang, "Review of wheeled mobile robots' navigation problems and application prospects in agriculture," *IEEE Access*, vol. 6, pp. 49 248–49 268, 2018.

[4] N. Sato, F. Matsuno, and N. Shiroma, "Fuma : Platform development and system integration for rescue missions," in *2007 IEEE International Workshop on Safety, Security and Rescue Robotics*, 2007, pp. 1–6.

[5] W.-T. Chen, E.-C. Tsui, W.-S. Yu, and P.-C. Lin, "Indoor and outdoor multi-terrain stair-climbing robot design," in *2025 IEEE International Conference on Robotics and Automation (ICRA)*, 2025, pp. 14 419–14 425.

[6] V. V. Vantsevich, D. J. Gorsich, J. R. Paldan, M. Ghasemi, and L. Moradi, "Terrain mobility performance optimization: Fundamentals for autonomous vehicle applications. part i. new mobility indices: Optimization and analysis," *Journal of Terramechanics*, vol. 104, pp. 31–47, 2022.

[7] E. Karpman, J. Kövecses, D. Holz, and K. Skonieczny, "Discrete element modelling for wheel-soil interaction and the analysis of the effect of gravity," *Journal of Terramechanics*, vol. 91, pp. 139–153, 2020.

[8] S. Shrivastava, A. Karsai, Y. O. Aydin, R. Pettinger, W. Bluethmann, R. O. Ambrose, and D. I. Goldman, "Material remodeling and unconventional gaits facilitate locomotion of a robophysical rover over granular terrain," *Science robotics*, vol. 5, no. 42, p. eaba3499, 2020.

[9] M. Bekker, "Theory of land locomotion: The mechanics of vehicle mobility," 1956.

[10] W. Li, J. Guo, L. Ding, J. Wang, and H. Gao, "Slippage-dependent teleoperation of wheeled mobile robots on soft terrains," *IEEE Robotics and Automation Letters*, vol. 6, no. 3, pp. 4962–4969, 2021.

[11] A. Ugenti, R. Galati, G. Mantriota, and G. Reina, "Analysis of an all-terrain tracked robot with innovative suspension system," *Mechanism and Machine Theory*, vol. 182, p. 105237, 2023.

[12] M. Raibert, K. Blankespoor, G. Nelson, and R. Playter, "Bigdog, the rough-terrain quadruped robot," *IFAC Proceedings Volumes*, vol. 41, no. 2, pp. 10 822–10 825, 2008.

[13] J. Lee, J. Hwangbo, L. Wellhausen, V. Koltun, and M. Hutter, "Learning quadrupedal locomotion over challenging terrain," *Science robotics*, vol. 5, no. 47, p. eabc5986, 2020.

[14] S. Choi, G. Ji, J. Park, H. Kim, J. Mun, J. H. Lee, and J. Hwangbo, "Learning quadrupedal locomotion on deformable terrain," *Science Robotics*, vol. 8, no. 74, p. eade2256, 2023.

[15] J. Chen, J. Frey, R. Zhou, T. Miki, G. Martius, and M. Hutter, "Identifying terrain physical parameters from vision - towards physical-parameter-aware locomotion and navigation," *IEEE Robotics and Automation Letters*, vol. 9, no. 11, pp. 9279–9286, 2024.

[16] H. Qi, L. Ding, M. Zheng, L. Huang, H. Gao, G. Liu, and Z. Deng, "Variable wheelbase control of wheeled mobile robots with worm-inspired creeping gait strategy," *IEEE Transactions on Robotics*, vol. 40, pp. 3271–3289, 2024.

[17] Y.-S. Kim, G.-P. Jung, H. Kim, K.-J. Cho, and C.-N. Chu, "Wheel transformer: A wheel-leg hybrid robot with passive transformable wheels," *IEEE Transactions on Robotics*, vol. 30, no. 6, pp. 1487–1498, 2014.

[18] S.-C. Chen, K.-J. Huang, W.-H. Chen, S.-Y. Shen, C.-H. Li, and P.-C. Lin, "Quattroped: A leg–wheel transformable robot," *IEEE/ASME Transactions on Mechatronics*, vol. 19, no. 2, pp. 730–742, 2014.

[19] T.-H. Wang, D.-G. Sung, and P.-C. Lin, "Terrain classification, navigation, and gait selection in a leg-wheel transformable robot by using environmental rgbd information," in *2018 International Automatic Control Conference (CACS)*, 2018, pp. 1–1.

[20] C. Li, T. Zhang, and D. I. Goldman, "A terradynamics of legged locomotion on granular media," *science*, vol. 339, no. 6126, pp. 1408–1412, 2013.

[21] F. Qian, T. Zhang, W. Korff, P. B. Umbanhowar, R. J. Full, and D. I. Goldman, "Principles of appendage design in robots and animals determining terradynamic performance on flowable ground," *Bioinspiration & biomimetics*, vol. 10, no. 5, p. 056014, 2015.

[22] S. Seok, A. Wang, M. Y. Chuah, D. J. Hyun, J. Lee, D. M. Otten, J. H. Lang, and S. Kim, "Design principles for energy-efficient legged locomotion and implementation on the mit cheetah robot," *IEEE/ASME Transactions on Mechatronics*, vol. 20, no. 3, pp. 1117–1129, 2015.